J Appl Electrochem (2009) 39:1349–1360
DOI 10.1007/s10800-009-9808-3

ORIGINAL PAPER

Direct electrolytic reduction of solid alumina using molten calcium chloride-alkali chloride electrolytes

Xiao Y. Yan · Derek J. Fray

Received: 18 September 2007 / Accepted: 21 January 2009 / Published online: 11 February 2009

Abstract Solid alumina was reduced by electro-deoxidation to aluminium metal containing 1.8 and 5.4 at% Ca in molten $CaCl_2$–NaCl and $CaCl_2$–LiCl electrolytes at 900 °C, respectively. The potential-pO^{2-} diagrams for the Al–O–M–Cl (M = Na or Li, or/and Ca) system were constructed to predict equilibrium phase relationships in the electrolytes at 700 and 900 °C. It was found that calcium aluminates were formed as the main intermediate reaction products and were subsequently reduced to form the Al-rich Al–Ca alloys during electro-deoxidation. Calcium and/or lithium, at reduced activities, were created at the cathode especially at 700 °C at the same time as the ionization of the oxygen from the cathode, which resulted in Al_2Ca formation. The experimental results were consistent with the thermodynamic predictions.

Keywords Electrolysis · Calcium chloride-alkali chloride electrolytes · Alumina · Reduction · Thermodynamic properties

1 Introduction

Aluminium and its alloys are widely used as structural and functional materials in transportation, packing, construction, electrical, and many other advanced applications. Primary Al is commercially produced by the Hall–Heroult process [1, 2]. The basic features have remained essentially unchanged since the process was developed more than 100 years ago, although significant optimization of process variables has taken place to cut production costs and reduce greenhouse gas emissions [3–6].

Possibilities of using alternate Al reduction processes have been investigated extensively over several decades to reduce overall production costs and to achieve environmental benefits. The alternative processes studied so far include [1, 2, 7, 8]: (i) carbothermic reduction of Al_2O_3 to Al, (ii) direct reduction of bauxite to Al–Si alloys, (iii) Bayer/Al_2O_3–C-anode in chloride electrolytes, (iv) electrolysis of aluminous ores/alloy separation and purification, (v) Bayer/carbochlorination/bipolar cell, (vi) carbochlorination of ore/separation and purification of metal chlorides/bipolar cell, and (vii) Bayer/carbonitridation or carbosulfidation/electrolysis of AlN or Al_2S_3.

In this paper, we describe an electro-deoxidation method and report a set of conditions under which the oxygen is electrochemically removed from solid Al_2O_3 or in situ formed aluminates by making the oxides the cathode in a bath of molten $CaCl_2$-based chlorides. The method of electro-deoxidation has been successfully used to produce many metals and alloys from their oxide precursors using the $CaCl_2$- and LiCl-based electrolytes [9–23]. In this work, solid Al_2O_3 acted as the cathode in molten $CaCl_2$-alkali chloride electrolytes. When potentials imposed to the cathode were more cathodic than oxygen ionization potentials of the Al_2O_3 or aluminates, but less cathodic than those needed for cathodic deposition of Ca or alkalis from the chloride electrolytes, the cathodic ionization of the oxygen from the oxides occurred through Reaction 1 rather than the cathodic deposition of the cations from the electrolytes due to Reaction 2:

X. Y. Yan (✉)
Division of Minerals, Commonwealth Scientific and Industrial Research Organisation, Clayton, VIC 3168, Australia
e-mail: yong.yan@csiro.au

D. J. Fray
Department of Materials Science and Metallurgy, University of Cambridge, Cambridge CB2 3QZ, UK

$$[\mathrm{O}](\text{in oxides}) + 2\mathrm{e} = \mathrm{O}^{2-}(\text{in electrolyte melt}) \quad (1)$$

$$\mathrm{M}^{n+}(\mathrm{M} = \mathrm{Na}\text{ or }\mathrm{Li}, \text{or}\,\mathrm{Ca}) + n\mathrm{e} = \mathrm{M}\,(n = 1\text{ or }2) \quad (2)$$

where [O] is the O in a solid Al_2O_3 or aluminate, M^{n+} and M are the metallic cation and the metal, respectively, and n is the number of electrons transferred. The ionized oxygen (O^{2-}) dissolved into the electrolyte, diffused from the cathode to the anode where it discharged, and the metal was left behind at the cathode. The anodic reactions with the carbon anode are given by

$$\mathrm{O}^{2-} - 2\mathrm{e} + 1/x\mathrm{C} = 1/x\mathrm{CO}_x(\mathrm{g}); \quad (x = 1\text{ or }2) \quad (3)$$

The overall cell reaction, by combining Reaction 1 with 3, may be simply as follows:

$$[\mathrm{O}](\text{in oxides}) + 1/x\mathrm{C} = 1/x\mathrm{CO}_x(\mathrm{g}); \quad (x = 1\text{ or }2) \quad (4)$$

2 Experimental

Fully dense Al_2O_3 tubes, of two different sizes (O.D. = 8 mm and I.D. = 5 mm; O.D. = 6 mm and I.D. = 4 mm, 99.8%, Ceramic Oxides Fabricators) were used as the starting material for Al_2O_3 cathodes. $CaCl_2 \cdot 2H_2O$ (greater than 99%, Aldrich) and anhydrous LiCl (99%, Sigma) were dehydrated in air at 150 °C for 1 h, heated at a rate of 6 °C h^{-1} to 350 °C, and then held at 350 °C for 12 h. A certain quantity of CaO may be generated during the drying process. The Li-saturated LiCl–Li melt was prepared by in situ electrolysis of molten LiCl at 700 °C until the LiCl–Li melt saturated with Li was produced. NaCl (at least 99.5%, Fluka) was dried in air at 120–150 °C for at least 5 h prior to use. Nb sheet (0.127 mm thick, 99.5%, Fansteel Inc.) was employed to fabricate a Nb basket for containing cathode materials. Figure 1 shows a schematic diagram of the electrolytic cell used in this work. High density graphite rods (Tokai Carbon Grade G347, 500 × 6 mmØ, Carbon Products of Australia; 100 × 10 mmØ, Graphite Technologies) were used as the anodes, respectively. An Al_2O_3 tube (O.D. = 10 mm and I.D. = 6.1 mm, 99.8%, Ceramic Oxides Fabricators) was used as the sheath for a certain section of the graphite rod anode. A stainless steel crucible was used to contain the molten salt electrolyte. Kanthal® wire (1 mmØ, Kanthal Australia Pty Ltd) and Ni wire (1.62 mmØ, Austral Wright Metals) were used as the electrode leads, respectively. The cell was placed inside a sealed Inconel reactor, which was continuously purged with dried high-purity argon throughout the experiments. The moisture and metallic impurities in the electrolytes were removed, while the quantities of CaO and Li_2O in the salts were very low and both of the oxides were also electrochemically decomposed to a great extent by pre-electrolysis between the graphite rod anode and the stainless steel crucible at a cell voltage of 2.8 V under the argon at 900 °C for 10 h or longer.

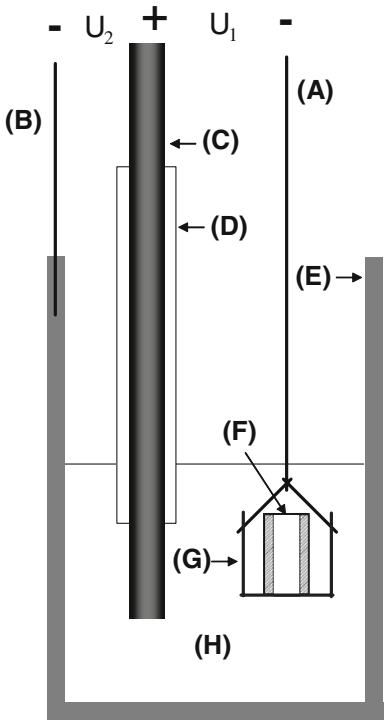

Fig. 1 Schematic diagram of the fused salt electrolytic cell used in this work (A. Kanthal wire, B. Ni wire, C. carbon anode, D. Al_2O_3 sheath, E. stainless steel crucible, F. Al_2O_3 tube, G. Nb basket, and H. fused salt electrolyte)

Electro-deoxidation was carried out at controlled potentials of 3.1 V at 900 °C and 3.4 V at 700 °C between the oxide cathode and the graphite rod anode, with a potential of 2.8 V being imposed between the crucible auxiliary cathode and the same carbon anode to prevent corrosion of the crucible. After electrolysis, the Nb basket was lifted to the top chamber of the reactor, allowing the cathode products to be argon-quenched and the salts remaining in the products to be solidified, thus preventing oxidation. The basket containing the cathode products was then taken out of the reactor at room temperature and was washed extensively in cold distilled water, followed by acetone rinse.

The cathode products were characterized using an optical microscope, a scanning electron microscope (SEM) with an energy dispersive spectrum (EDS) and energy dispersive X-ray (EDX) analysis, inductively coupled plasma (ICP), and X-ray diffractometry (XRD).

3 Results and discussion

A $CaCl_2$–NaCl melt containing 32.2 mol% NaCl and an equimolar $CaCl_2$–LiCl mixture were used as the

electrolytes for electro-deoxidation of solid Al_2O_3. $CaCl_2$ was chosen as the major component of the electrolytes due to its several desirable properties: very high solubility for O^{2-} (e.g., 20 mol% CaO in $CaCl_2$ at 900 °C [24]), extremely high solubility of $CaCl_2$ in water (1.59 g mL^{-1} of H_2O), low cost, very low toxicity, and ready availability. The addition of NaCl or LiCl to molten $CaCl_2$ can lower liquidus temperatures and increase electrical conductivities of the electrolytes [25].

3.1 Thermodynamic considerations

Thermodynamic properties in the Al–O–M–Cl (M = Na or Li, or/and Ca) system at 700 and 900 °C are represented using the predominance diagrams on which the processes of electro-deoxidation are critically evaluated. The method of constructing the diagrams from pertinent thermodynamic data was based on those described by Littlewood [26], where the equilibrium potential E (relative to the standard chlorine electrode, S.Cl.E.) is plotted against the activity of O^{2-} expressed as its negative logarithm, pO^{2-}, in the chloride melts for Al. The E-pO^{2-} diagrams summarise chemical and electrochemical properties of Al in the electrolytes at a given temperature as a function of pO^{2-}, from which equilibrium phase relationships in the oxide/metal/salt systems can be better understood.

Ferry et al. used the E-pO^{2-} diagrams of Fe–Ti–O compounds in molten LiCl–KCl eutectic at 470 °C to predict operating conditions for selective chlorination of TiO_2 and subsequent electrowinning of metallic Ti in the melts [27]. The E-pO^{2-} diagram for the Ti–O system at 550 °C was recently made by Martinez et al. to study the chemical and electrochemical properties of solutions of Ti chlorides in an equimolar $CaCl_2$–NaCl mixture [28]. More recently, Inman et al. constructed the predominance diagrams for studying the direct electrochemical reduction of solid TiO_2 and mixed oxide precursors in molten $CaCl_2$ at around 900 °C [29–31]. Yasuda et al. utilized the E-pO^{2-} diagram of Si in molten $CaCl_2$ at 850 °C to study the direct electrolytic reduction of SiO_2 [32]. The E-pO^{2-} diagrams of Al in molten LiCl–KCl eutectic at 470 °C have been constructed by Picard et al. to investigate the chlorination of Al_2O_3 in molten salts [33–35]. In their diagrams, complex oxides of Al and Li were excluded. Little has been reported so far on the E-pO^{2-} diagrams of Al in $CaCl_2$–NaCl and $CaCl_2$–LiCl melts at 700 and 900 °C, including various aluminates.

Construction of E-pO^{2-} diagrams requires the definitions of standard states for the species involved. For the present systems, they are described as follows: (i) pure solid invariant compounds have unit activities, (ii) CaO at unit activity is denoted as an O^{2-} activity of one, (iii) pure O_2 or Cl_2 gas at 1 atm is taken as its standard state, (iv) Ca or alkalies at unit activity is regarded as its standard state, and (v) metal chloride at unit activity is chosen as the standard state for its cation, e.g., pure $CaCl_2$ is selected as the standard state for Ca^{2+}. In the following E-pO^{2-} diagrams, diagonal dot lines are iso-pressure lines for O_2 (p_{O_2}) in the gaseous phase in equilibrium with chloride melt, while horizontal dot lines are iso-activity lines where a_{Ca} and a_{Li} are the activities of Ca and Li dissolved in their chlorides, respectively, and a_{Ca} [$Al_2Ca(s)$], a_{Ca} [$Al_4Ca(s)$], and a_{Li} [AlLi(s)] are the activities of Ca and Li in molten $CaCl_2$ and LiCl in equilibrium with $Al_2Ca(s)$, $Al_4Ca(s)$ and AlLi(s), respectively.

3.1.1 Combined E-pO^{2-} diagrams of Al in molten $CaCl_2$ and a $CaCl_2$–NaCl melt containing 32.2 mol% NaCl at 700 and 900 °C

CaO is soluble in molten $CaCl_2$-based salts, e.g., 18 mol% CaO in molten $CaCl_2$ and 15 mol% CaO in molten $CaCl_2$–NaCl mixture containing 32.2 mol% NaCl at 850 °C [24, 36]. However, solubilities of Na_2O and CaO in molten NaCl are negligibly small [37, 38]. An inspection of the Al_2O_3–CaO phase diagram shows that Al_2O_3 and CaO form a series of Ca aluminates in the Al_2O_3-rich region [39]. Ca aluminates are likely to form through chemical reactions between solid Al_2O_3 and CaO in $CaCl_2$-based electrolytes and are thus considered in the construction of the E-pO^{2-} diagrams. There are no available activity data for NaCl and $CaCl_2$ in molten $CaCl_2$–NaCl solutions at 700 and 900 °C in the literature. However, Chartrand and Pelton reported that molten $CaCl_2$–NaCl solutions exhibit negative deviations from ideality at 825 and 850 °C, respectively, and changes in temperature have little influence on NaCl activities over the entire composition range [40]. It is therefore reasonable to assume that there is no temperature dependence of NaCl activity in the solutions between 700 and 900 °C. It is further assumed that molten $CaCl_2$–NaCl solutions behave regularly. Activities of $CaCl_2$ and NaCl in the $CaCl_2$–NaCl melt containing 32.2 mol% NaCl at 700–900 °C are thus calculated to be 0.582 and 0.163, respectively, using the relevant activity data [40]. Decomposition potentials of the present $CaCl_2$–NaCl melt can be then calculated from the calculated activities at 700 and 900 °C, respectively.

Figure 2a, b shows combined E-pO^{2-} diagrams of Al in molten $CaCl_2$ (dashed line) and a melt of $CaCl_2$–NaCl containing 32.2 mol% NaCl (solid line) at 700 and 900 °C, respectively, as constructed using thermodynamic data [33, 40, 41]. At both temperatures, the addition of NaCl to molten $CaCl_2$ slightly widens the electrochemical window owing to decreasing $CaCl_2$ activity, but this effect is likely to be offset by cathodic deposition of Ca–Na alloys. As can be seen from Fig. 2, chemical interactions between Al_2O_3 and dissolved CaO to produce Ca aluminates require higher

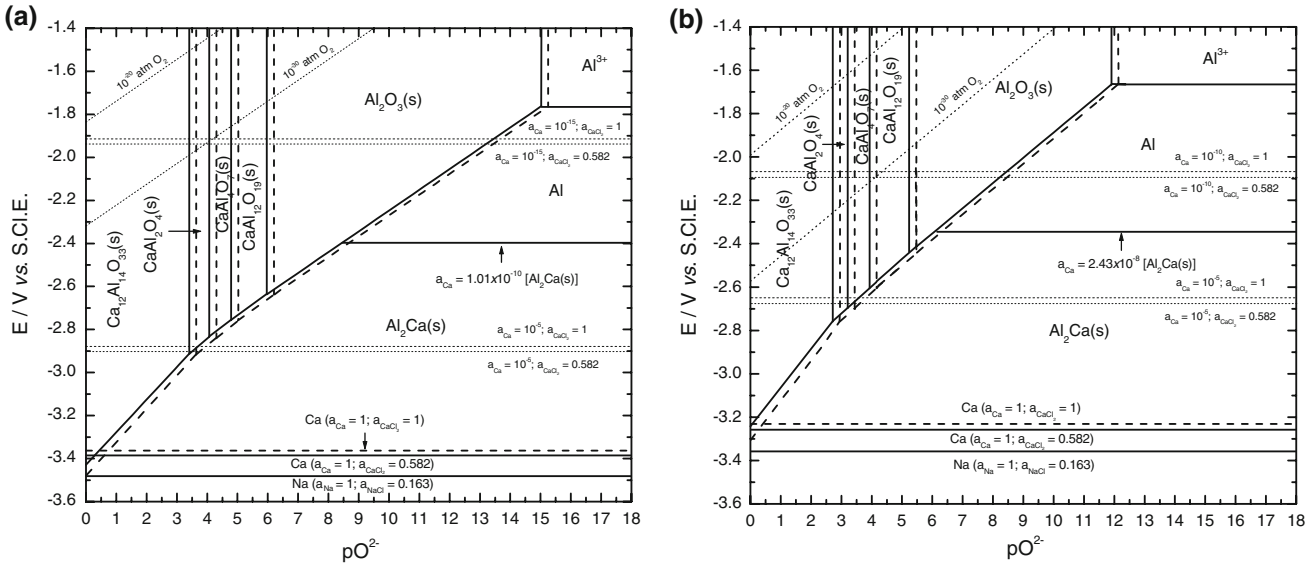

Fig. 2 Combined potential-pO^{2-} diagrams of Al in molten $CaCl_2$ and a $CaCl_2$–NaCl melt containing 32.2 mol% NaCl at **a** 700 °C and **b** 900 °C

activities of O^{2-}, i.e., lower pO^{2-} values, in the $CaCl_2$–NaCl compared to molten $CaCl_2$. It can also be seen that solid Al_2O_3 or Ca aluminates are likely to reduce to metallic Al and Al_2Ca or Al_2Ca alone at less cathodic potentials in the $CaCl_2$–NaCl melt than molten $CaCl_2$, depending on cathodic potential and O^{2-} activity. The formation of Al_2Ca is more favourable than metallic Al over low pO^{2-} regions. As an example, both Al_2O_3 and Ca aluminates can be reduced to form Al_2Ca only at a cathodic potential of 3.1 V versus S.Cl.E. over the pO^{2-} region of 0.3–8.5 at 700 °C or 0–6.1 at 900 °C in the $CaCl_2$–NaCl melt. Furthermore, it is important to note that all oxides become more stable as temperature decreases. For instance, $Ca_{12}Al_{14}O_{33}$ is even thermodynamically more stable than the $CaCl_2$–NaCl melt at pO^{2-} values less than 0.3 at 700 °C. Similarly, pO^{2-} regions where $Ca_{12}Al_{14}O_{33}$ is more stable than the electrolytes under other conditions can also be read from Fig. 2.

3.1.2 *Combined E-pO^{2-} diagrams of Al in molten $CaCl_2$ and a LiCl melt at 700 and 900 °C*

Li_2O has appreciable solubilities in molten LiCl, e.g., 16 mol% Li_2O in molten LiCl at 750 °C [42], whereas solubilities of CaO in molten LiCl are very low, e.g., 0.44–0.96 mol% CaO at 700–900 °C [38]. Wang et al. reported that the solubility of CaO in an equimolar $CaCl_2$–LiCl melt is 13.32 mol% CaO at 750 °C [43]. Hence, Li_2O dissolved in molten LiCl or an equimolar $CaCl_2$–LiCl melt is likely to react with solid Al_2O_3 to produce Li aluminates, as predicted from the Al_2O_3–Li_2O phase diagram [39]. Due to the lack of thermodynamic data for $LiAl_5O_8$, this phase is thus excluded in *E*-pO^{2-} diagrams of Al in molten LiCl. Figures 3a and b show combined *E*-pO^{2-} diagrams of Al in molten $CaCl_2$ (solid line) and LiCl (dashed line) at 700 and 900 °C, respectively. It can be seen from Fig. 3 that Al_2O_3 is more stable in molten LiCl than $CaCl_2$ and thermodynamic stabilities of $LiAlO_2$ are much higher than Ca aluminates at 700 or 900 °C. The stabilities for all the oxides increase, but the activities of Ca in the melt required to form solid Al_2Ca become much smaller with decreasing temperature. It can be further seen that $LiAlO_2$ is thermodynamically more stable than molten LiCl when the values of pO^{2-} are less than 2.2 at 700 °C and 1.8 at 900 °C.

From a thermodynamic viewpoint, solid Al_2O_3 and Ca aluminates may be electro-deoxidized to metallic Al and/or Al_2Ca over certain regions of pO^{2-} values at imposed cell voltages of 3.4 V at 700 °C and 3.1 V at 900 °C. Cl^- ions from a chloride electrolyte are unlikely to be discharged at the carbon anode as the potential for Cl_2 evolution is considerably more anodic than evolution of CO or CO_2, as shown in Fig. 3. Moreover, it is more difficult to electro-deoxidize the oxides and it is more favourable to form Al_2Ca at 700 °C than 900 °C.

3.2 Electrolytic reduction of solid Al_2O_3

In this work, the progress of reaction is described by the extent of reduction (X) defined as follows:

$$X = \frac{W^0 - W^t}{W^0} \times 100\% \quad (5)$$

where X is the extent of reduction, W^0 is the mass of oxide (Al_2O_3) at the beginning ($t = 0$), and W^t is the mass of oxide or oxides at time t. A series of electrolysis

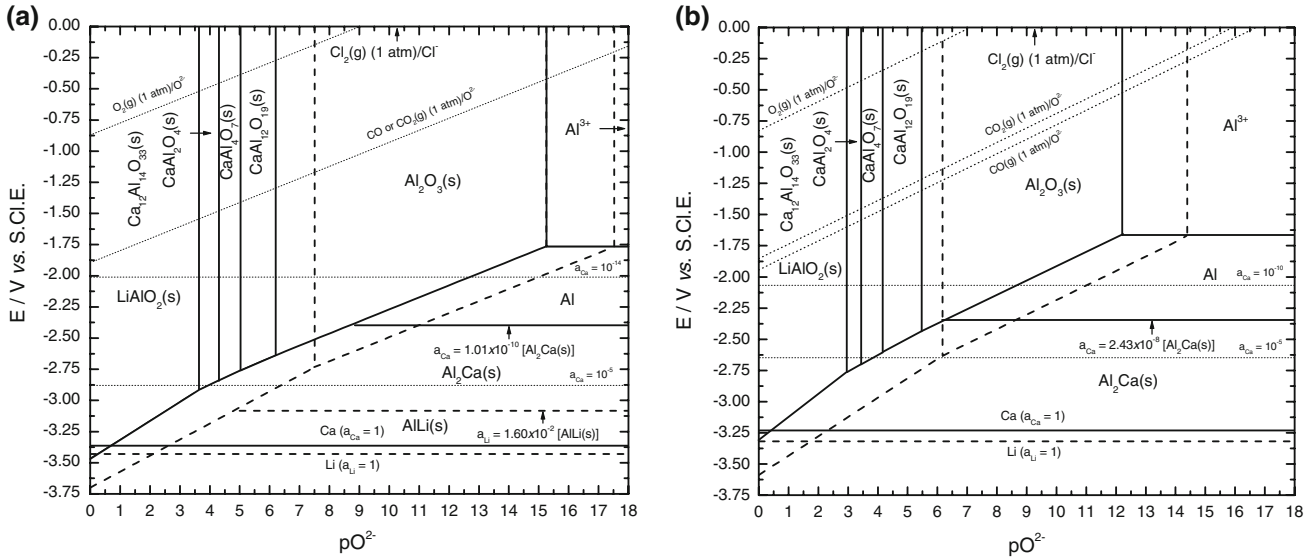

Fig. 3 Combined potential-pO^{2-} diagrams of Al in molten $CaCl_2$ and a LiCl melt at **a** 700 °C and **b** 900 °C

experiments were undertaken under various conditions to investigate key factors influencing the direct electrolytic reduction of solid Al_2O_3. The experimental conditions used and the values of X obtained are given in Table 1.

Figure 4 shows the typical current-time curve measured at the early stage of electrolysis of the fully dense tube of Al_2O_3* in the fused $CaCl_2$–NaCl electrolyte containing 32.2 mol% NaCl at 900 °C (run 1). It was found from Fig. 4 that the currents, on the application of 3.1 V, jumped to a value of 0.9 A and then decayed rapidly, followed by steady current decline with time, approaching the residual values of around 0.2 A after 15 h electrolysis. This is similar to the current-time behaviours reported for direct electrochemical reduction of SiO_2 and TiO_2 in molten $CaCl_2$ at 850 °C [16, 23]. Cowley reported that solubilities of Ca–Na alloys in approximately equimolar $CaCl_2$–NaCl melts are 0.4–4.5 wt% Na, increasing with increasing temperature, and the Ca–Na alloys contain at least 98 at% Na at 500–700 °C [44]. Dissolution of elemental Ca and Na into the $CaCl_2$–NaCl melt imparted certain degrees of electronic conductance to the melt [45]. The observed residual currents were due to small amounts of dissolved Ca and Na being generated during electrolysis. Moreover, solid Al_2O_3 is regarded as an electrical insulator since its electrical resistivity is $2 \times 10^4\ \Omega$ m at 1,000 °C [46]. Consequently, the cathodic ionization of the oxygen from the Al_2O_3 exposed to the electrolyte was restricted to the Al_2O_3/electrolyte/Nb three phase boundaries (3PBs) at 3.1 V.

Table 1 The present experimental conditions used for electrolytic reduction of solid Al_2O_3 in molten metal chlorides and the extents of reduction obtained

Run no.	Electrolysis conditions					X (%)
	Cathode material/initial weight (g)	Electrolyte	U_1 (V)	T (°C)	t (h)	
1	Al_2O_3*/1.939	$CaCl_2$–NaCl	3.1	900	66	24
2	Al_2O_3/0.633	$CaCl_2$–LiCl	3.1	900	23.7	78
3	Al_2O_3/0.69	$CaCl_2$–NaCl	3.1	900	23.33	71
4	Al_2O_3/0.649	$CaCl_2$–NaCl	3.4	700	23.33	35
5	Al_2O_3/0.679	$CaCl_2$–LiCl	3.4	700	24	100
6	Al_2O_3/0.673	$CaCl_2$–LiCl	3.4	700	23.7	100
7	Al_2O_3/0.648	LiCl	3.4	700	29.75	0
8	Al_2O_3/0.61	LiCl–Li	3.4	700	4	8
9	Al_2O_3/0.646	LiCl–Li	3.4	700	20	15

Notes: The inner and outer diameters of the Al_2O_3 tubes used were 4 and 6 mm, respectively, except for the Al_2O_3* tube that had 5 mm in inner diameter and 8 mm in outer diameter

$CaCl_2$–NaCl and $CaCl_2$–LiCl are a $CaCl_2$–NaCl melt containing 32.2 mol% NaCl and an equimolar $CaCl_2$–LiCl melt, respectively

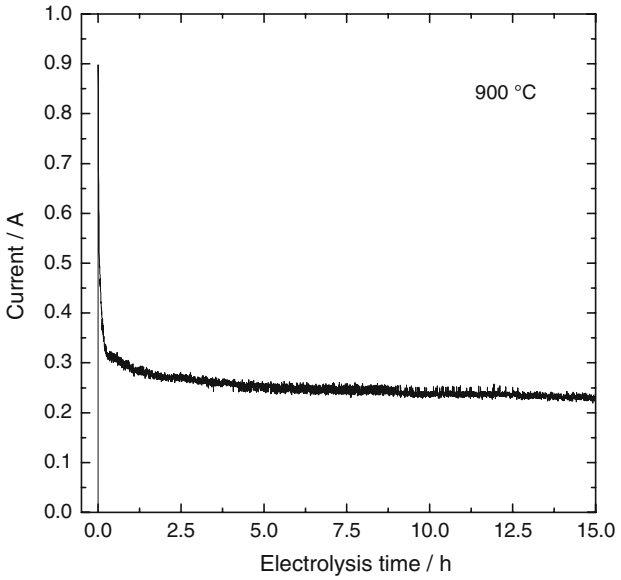

Fig. 4 Current–time curve of the Al_2O_3 tube during electro-deoxidation at 3.1 V in the molten $CaCl_2$–NaCl electrolyte containing 32.2 mol% NaCl at 900 °C

Figure 5 shows the photographs of (a) the Al_2O_3 tubes before and after electrolysis (run 1), (b) the metal droplets collected from the Nb basket after 66 h electrolysis, and (c) the inner surface of the Nb sheet employed for fabricating the basket after electrolysis, respectively. As observed from Fig. 5a, the size of the Al_2O_3 tube diminished in three dimensions after electrolysis, implying that electronically conducting phases had formed on the Al_2O_3 surface which subsequently acted as electron transfer medium for the electro-deoxidation to occur not only at the 3PBs of the oxide/electrolyte/Nb but also at the oxide/electrolyte interface. As a result, the reduction spread along the surface of the tube and then into the interior. Ionized O^{2-} dissolved into the electrolyte and liquid Al formed which spheroidized and the droplets fell from the tube to the basket bottom. It is also observed from Fig. 5b that the nearly spherical droplets collected had droplet sizes ranging from several hundred microns to about 2 mm, indicative of coalescence amongst the initial small-sized droplets during electrolysis. EDS spectra of the droplet surfaces showed predominant peaks for Al and a very weak peak for O, indicating that the surface material was Al. Figure 5c shows that some droplets had reacted with the Nb basket, forming new phases consisting of Al and Nb (marked by A) on the inner surface of the Nb basket (marked by B).

The above results confirmed that the electrolytic reduction of the oxides to liquid Al was responsible for the current–time behaviour in Fig. 4. The value of X, as determined from the measured mass change of the Al_2O_3 before and after electrolysis, was calculated to be 24%

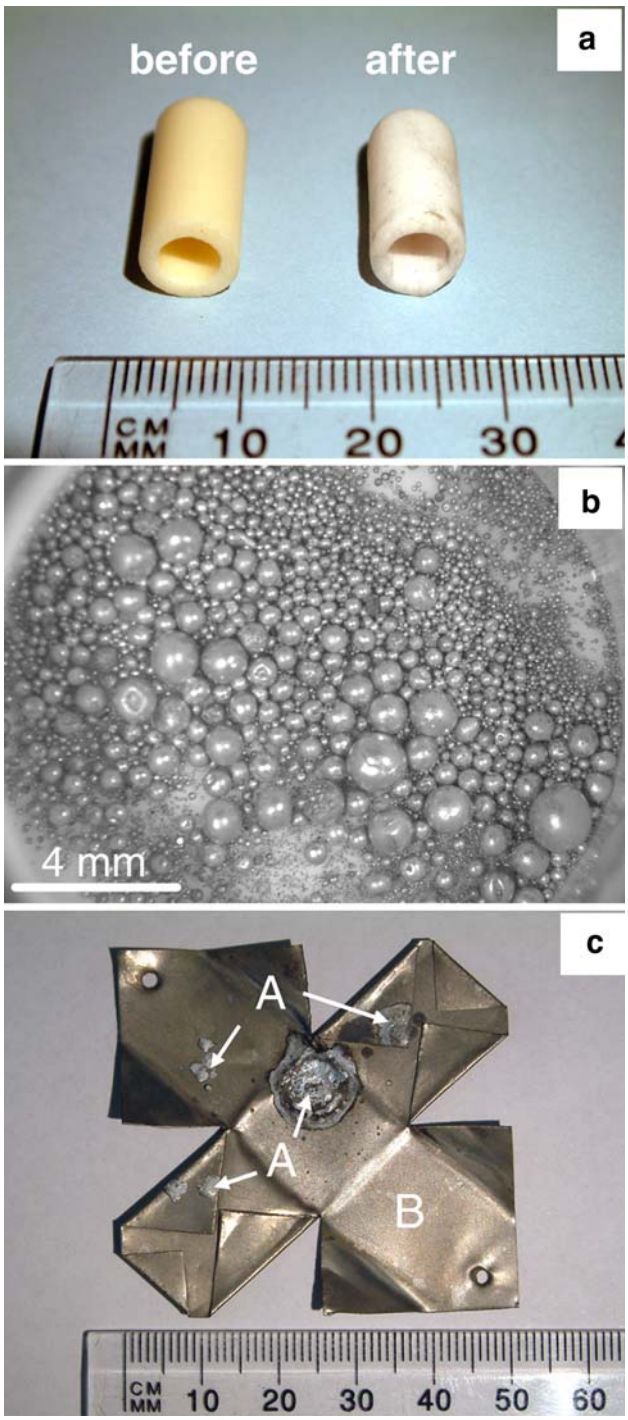

Fig. 5 Photographs of **a** the dense tubes of Al_2O_3 before and after 66 h electrolysis in the $CaCl_2$–NaCl melt consisting of 32.2 mol% NaCl at 900 °C (run 1), **b** the reduced Al droplets collected from the Nb basket after electrolysis, and **c** the Nb sheet used for fabricating the Nb basket after electrolysis

according to Eq. 5. In this work, the cathodic current efficiency was defined by a percentage of the measured mass change in O content of an oxide cathode before and after electrolysis compared to the total O mass change

evaluated from the measured current–time curve. The cathodic current efficiency over the period of 66 h electrolysis was determined to be about 25% after the residual current subtraction.

Figure 6a illustrates the SEM backscattered electron (BE) micrograph of the polished cross section of one of the droplets in Fig. 5b. The droplet is characterized by distinct gray and bright areas, typical of microstructure of the eutectic-type alloys, and is fully covered with a grey layer. Figure 6b is the enlarged SEM-BE image of that in Fig. 6a, clearly showing that the large grey areas marked by A is surrounded by mixed grey and bright areas marked by B.

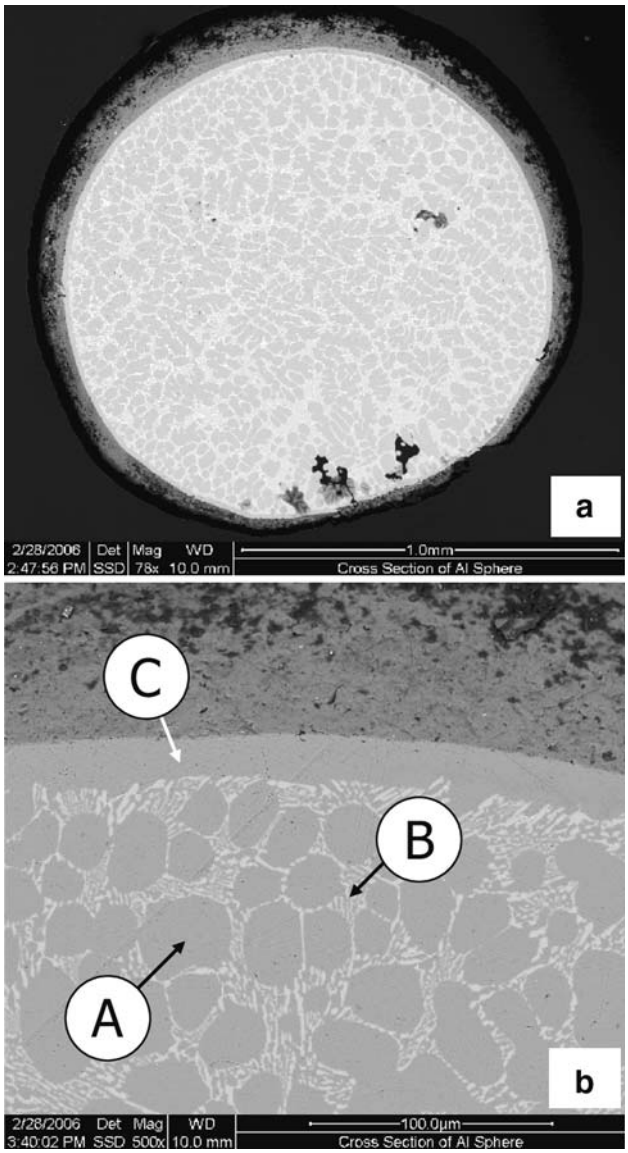

Fig. 6 SEM backscattered electron (BE) images of **a** the polished cross section of the reduced Al droplet in Fig. 5b and **b** enlarged SEM-BE image of the polished cross section of the Al droplet taken from the top part of the image in Fig. 6**a**

An EDX analysis of the layer marked C and the grey areas gave 98 at% Al and 2 at% O, while the mixed grey and bright areas had 81 at% Al, 17 at% Ca, and 2 at% O. As evaluated from the Al–Ca phase diagram [47], Al should co-exist with Al_4Ca (20 at% Ca) at temperatures below 613 °C. Therefore, the mixed grey and bright areas correspond to a mixture of the Al and Al_4Ca, with the detected O stemming from surface oxidation of the sample at room temperature. Elemental Na was not detected by EDS and EDX analyses of all the areas within the sample in Fig. 6a.

The overall composition of the remaining droplets in Fig. 5b, as determined by ICP, was 98.2 at% Al and 1.8 at% Ca. The ICP result confirmed that the oxides had been reduced to Al-rich Al–Ca alloys at 900 °C. With the overall Ca content (1.8 at% Ca) being far less than that in Al_2Ca (33 at% Ca), it is believed that the reduction of the oxides proceeds in the electrolyte where activities of the dissolved Ca are less than 2.43×10^{-8}, as predicted from Fig. 2b; otherwise, the Ca dissolved in the electrolyte in equilibrium with solid Al_2Ca would diffuse into the reduced Al driven by differences in Ca chemical potential between the electrolyte and Al to produce Al_2Ca. Reaction 1 is hence predominant at the cathode. During cooling of the cathode products after electrolysis, the solid Al_4Ca and Al are precipitated from the Al-rich Al–Ca melt, leading to the observed eutectic-type alloy microstructure in Fig. 6.

3.3 Intermediate reaction products

Figure 7a shows the SEM-BE micrograph of the polished cross section of the small Al_2O_3 tube electrolysed in the equimolar $CaCl_2$–LiCl melt at 900 °C (run 2), from which it can be clearly observed that the un-reduced core was fully covered with a dense layer. An EDS analysis of several spots within the core and the layer revealed that the core remained as Al_2O_3, while the layer was composed of elemental Al, Ca, O, and Cl. Figure 7b shows the enlarged SEM-BE image taken from a portion of the layer in Fig. 7a. As observed from Fig. 7b, the layer actually consists of grey areas, bright grey areas, and bright areas, as marked by A, B, and C, respectively. The EDX data measured from the different spots of the individual areas are given in Table 2. Elemental Li has an atomic weight too small to be detected by EDS and EDX. These results indicate the formation of aluminates within the layer. EDS analysis was also performed on the cross section of the layer on the Al_2O_3 after electrolysis in the $CaCl_2$–NaCl melt (run 3). The obtained EDS spectra, in this case, exhibited peaks for elemental Al, Ca, O, and Cl, but no peaks for elemental Na within the layer.

Figure 8 shows the XRD spectrum of the isolated layer on the Al_2O_3 tube in Fig. 7, which reveals that the layer consists

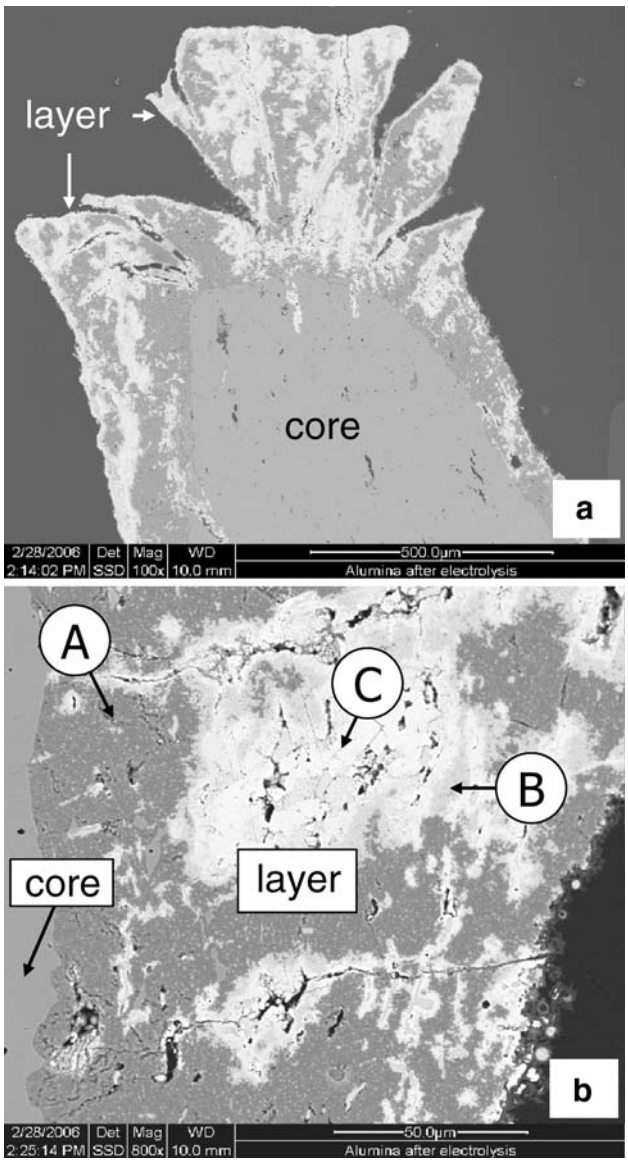

Fig. 7 SEM backscattered electron (BE) images of **a** the polished cross section of the remaining part of the Al_2O_3 tube after 23.7 h electrolysis in the equimolar melt of $CaCl_2$–LiCl at 900 °C (run 2) and **b** enlarged SEM-BE image showing a portion of the layer formed on the core of the un-reduced Al_2O_3 tube in Fig. 7**a**

Table 2 An EDX analysis of the elemental compositions on the layer of the Al_2O_3 tube after electrolysis in the molten equimolar $CaCl_2$–LiCl electrolyte at 900 °C for 23.7 h (run 2)

Area within the layer	Elemental composition range (at%)		
	Al	Ca	O
Gray area (marked by A)	88–79	1–2	10–20
Bright gray area (marked by B)	26–72	5–19	23–55
Bright area (marked by C)	25–26	18–19	55–57

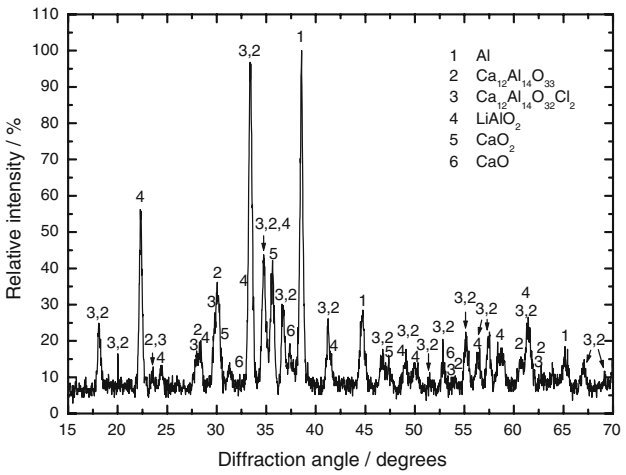

Fig. 8 XRD spectrum of the layer formed on the Al_2O_3 tube after electrolysis in the equimolar $CaCl_2$–LiCl electrolyte at 900 °C (run 2)

of metallic Al, $Ca_{12}Al_{14}O_{33}$, and $Ca_{12}Al_{14}O_{32}Cl_2$ as the major phases, $LiAlO_2$ as the medium phase, and CaO or CaO_2 as the trace or minor phase, free of Al_2O_3. These are to be expected as the standard Gibbs free energy change for the reaction of a Na aluminate with $CaCl_2$ to form a Ca aluminate and NaCl is negative at 900 °C. For example, $Na_2Al_2O_4 + CaCl_2 = CaAl_2O_4 + 2NaCl$, $\Delta G^0_{1173K} = -99.271\ kJ\ mol^{-1}$ should take place at 900 °C, with the equilibrium constant $k_p = 2.633 \times 10^4$[41]. In contrast, the standard Gibbs free energy change for the reaction of $LiAlO_2$ with $CaCl_2$ to form $CaAl_2O_4$ and LiCl is only slightly negative ($\Delta G^{\circ}_{1173K} = -4.087\ kJ\ mol^{-1}$), with a value of $k_p = 1.52$ at 900 °C [41]. The XRD result confirms that the aluminates were formed in situ on the Al_2O_3 surface and were then electro-deoxidized to Al-rich Al–Ca alloys mostly at the aluminate/electrolyte interfaces. $Ca_{12}Al_{14}O_{32}Cl_2$ and partially reduced Ca aluminates are electronic conductors [48–50]. For example, a partially reduced single crystal of $Ca_{12}Al_{14}O_{33}$ has an electronic conductivity of about 1 S m^{-1} at 27 °C [48]. The presence of very fine Al droplets maximises the 3 PB contact between the aluminate/electrolyte/Al within the layer, thus promoting electro-deoxidation. An advancing Al_2O_3/electrolyte reaction front to form the aluminates moves inwards and the un-reacted Al_2O_3 core shrinks continuously as the electro-deoxidation progresses, with the fine liquid Al coalescing, resulting in large droplets falling from the tube surface.

According to Figs. 2 and 3, the magnitude of pO^{2-} should determine which aluminate is stable within the layer on the Al_2O_3 surface in contact with electrolyte. The $CaCl_2 \cdot 2H_2O$ and anhydrous LiCl after thermal drying in air contained about 0.595 mol% CaO and 1.77×10^{-3} mol% Li_2O, respectively, as measured using the standard acid-base titration method. Mole fractions of CaO are

then calculated to be 4.03×10^{-3} in the $CaCl_2$–NaCl melt containing 32.2 mol% NaCl and approximately 2.98×10^{-3} in the equimolar $CaCl_2$–LiCl melt when neglecting the initial Li_2O amount in the LiCl. The Henrian activity coefficients of CaO ($\gamma_{(CaO)}$) as a function of temperature were recently determined experimentally by Wang et al. for molten $CaCl_2$ and equimolar $CaCl_2$–NaCl and $CaCl_2$–LiCl melts saturated with CaO [43]. The temperature dependence of $\gamma_{(CaO)}$ obtained by Wang et al. may be applicable to dilute solutions of CaO in the molten salts by assuming that $\gamma_{(CaO)}$ is independent of CaO concentration (Henry's law) and changes in NaCl concentration from 50 mol% to 32.2 mol%. The extrapolated values of $\gamma_{(CaO)}$ in the $CaCl_2$–NaCl melt were calculated according to their equations [43] to be 13.71 at 700 °C and 12.59 at 900 °C, while those in the equimolar $CaCl_2$–LiCl melt were 1.41 at 700 °C and 1.36 at 900 °C. Thus, the values of pO^{2-} before pre-electrolysis were estimated at 1.26 at 700 °C and 1.29 at 900 °C in the $CaCl_2$–NaCl melt and were 2.38 at 700 °C and 2.29 at 900 °C for the equimolar $CaCl_2$–LiCl melt. The calculations show that it is thermodynamically possible for CaO in the present electrolytes without pre-electrolysis to react with Al_2O_3 to produce $Ca1_2Al_{14}O_{33}$ or $Ca_{12}Al_{14}O_{33}$ and $LiAlO_2$ over these pO^{2-} regions, as predicted from Figs. 2 and 3. However, the CaO or Li_2O dissolved in the electrolytes are decomposed to evolve CO/C_2 gases at the carbon anode and to deposit cathodically metallic Ca or Li at the surface of the stainless steel crucible exposed to the electrolytes during pre-electrolysis at 2.8 V. The reduced Ca or Li subsequently dissolves in the $CaCl_2$-based electrolytes. The amount of the Ca or Li reduced from its oxide initially present in the salt is very low because of the very low quantities of initial oxide in the thermally dried salt. The electrochemical removal of the O^{2-} dissolved initially in the electrolytes by pre-electrolysis significantly reduced the O^{2-} activities, thus increasing values of pO^{2-} in the electrolytes.

From the thermodynamic predictions and observation of the various phases present in the products it can be concluded that the following reactions take place:

$$21/2Al_2O_3 + 12CaO + 21/2C = 7Al + Ca_{12}Al_{14}O_{33} + 21/2CO(g) \quad E^{o}_{1173K} = -0.962\ V[41] \tag{6}$$

$$Ca_{12}Al_{14}O_{33} + 21C = 14Al + 12CaO + 21CO(g) \quad E^{\circ}_{1173K} = -1.222\ V[41] \tag{7}$$

Li aluminate may also be formed by the reaction

$$3/2Al_2O_3 + Li_2O + 3/2C = Al + 2LiAlO_2 + 3/2CO_{(g)} \quad E^{\circ}_{1173K} = -0.701\ V[41] \tag{8}$$

and can be decomposed by the reaction:

$$2LiAlO_2 + 3C = 2Al + Li_2O + 3CO(g) \quad E^{\circ}_{1173K} = -1.352\ V[41] \tag{9}$$

The potentials for these reactions can be compared with the potential for the reduction of CaO:

$$CaO + C = Ca + CO(g) \quad E^{\circ}_{1173K} = -1.535\ V[41] \tag{10}$$

3.4 Factors affecting reduction behaviour

3.4.1 Effect of Al_2O_3 surface area

The specific surface area of the small Al_2O_3 tubes employed in run 3 was calculated to be 5.2×10^{-4} m^2 g^{-1}, greater than that of the large Al_2O_3* tube (3.5×10^{-4} m^2 g^{-1}) as used in run 1. As given in Table 1, the magnitudes of X achieved were 24% for run 1 and 71% for run 3. It was found that a 33% rise in specific surface area of the Al_2O_3 tubes led to an increase in the X value by 66%, although the electrolysis duration of run 3 was almost three times shorter than that of run 1. The findings suggested that the electro-deoxidation could be effectively enhanced by enlarging specific surface area of solid Al_2O_3.

3.4.2 Effect of electrolyte system

Table 1 shows that the value of X for run 2 using the equimolar $CaCl_2$–LiCl electrolyte was 78% and was only slightly higher than $X = 71\%$ from run 3 with the $CaCl_2$–NaCl electrolyte. The results indicate that the use of the $CaCl_2$–LiCl electrolyte has no obvious enhancement effect on the overall rate of electrolytic reduction of Al_2O_3 compared to that of $CaCl_2$–NaCl electrolyte at 900 °C under these conditions. The metallic droplets collected after run 2 had similar sizes to those from run 1 or 3 and they were actually Al-rich Al–Ca alloys containing 5.4 at% Ca on average, as determined by ICP. This amount of Ca was higher than that in the Al produced from run 1, although the initial CaO content (0.298 mol% CaO) in the equimolar $CaCl_2$–LiCl melt was lower than that (0.403 mol% CaO) in the $CaCl_2$–NaCl melt used in this work. This is probably due to two factors. First, the dissolved O^{2-} is predominantly associated with the Ca^{2+} as (CaO) instead of Na^+ as (Na_2O) or Li^- as (Li_2O) in the electrolytes:

$$(Na_2O) + CaCl_2 = (CaO) + 2NaCl \quad \Delta G^{o}_{1173K} = -203.859\ kJ\ mol^{-1}[41] \tag{11}$$

$$(Li_2O) + CaCl_2 = (CaO) + 2LiCl \quad \Delta G^{o}_{1173K} = -52.304\ kJ\ mol^{-1}[41] \tag{12}$$

where (CaO), (Na_2O), and (Li_2O) are the CaO, Na_2O, and Li_2O dissolved in the electrolyte melts, respectively. The equilibrium constants (k_p) for Reactions 11 and 12 at 900 °C are 1.196×10^9 and 2.133×10^2 [41], respectively,

indicating that the activities of Li_2O and especially Na_2O should be much lower than that of CaO in the electrolytes. The CaO dissolved in the electrolytes then reduces to metallic Ca at reduced activity through Reaction 10 during electrolysis and the reduced Ca subsequently dissolves in the $CaCl_2$-based electrolyte since Ca is soluble in molten $CaCl_2$ (2.1–3.6 mol% Ca in molten $CaCl_2$ at 800–940 °C [51]). Second, equilibria between (Ca) and (Na) in the $CaCl_2$–NaCl melt and between (Ca) and (Li) in the equimolar $CaCl_2$–LiCl melt may be governed by the following exchange reactions:

$$(Ca) + 2NaCl = 2(Na) + CaCl_2 \quad (13)$$

$$(Ca) + 2LiCl = 2(Li) + CaCl_2 \quad (14)$$

where (Ca), (Na), and (Li) are the Ca, Na, and Li dissolved in molten $CaCl_2$–NaCl and $CaCl_2$–LiCl mixtures, respectively. Solubilities of Na in molten NaCl are 2.8–10.2 mol% Na at 809–890 °C [52], while those of Li in molten LiCl range from 0.66 mol% to 1.22 mol% Li at 662–850 °C [53]. The equilibrium constants (k_p) for Reaction 13 are 44.66 at 700 °C and 59.17 at 900 °C, whereas the values of k_p for Reaction 14 are only 1.91×10^{-2} at 700 °C and 1.335×10^{-2} at 900 °C [41]. These indicated that activities of the Ca dissolved in the equimolar $CaCl_2$–LiCl melt are much higher than those in the $CaCl_2$–NaCl melt used. The higher activities of the Ca dissolved in the $CaCl_2$–LiCl melt cause the observed higher Ca content in the reduced Al. Nevertheless, the Ca activity in the $CaCl_2$–LiCl melt is still below a_{Ca} $[Al_2Ca(s)] = 2.43 \times 10^{-8}$ under the present conditions according to Fig. 3b. Although Na activities in the $CaCl_2$–NaCl melt might be greater than those of Ca, elemental Na was undetectable by EDS or EDX in the Al reduced using this electrolyte, probably because of the very low Na solubilities in liquid Al (e.g., about 0.18 at% Na in molten Al at 665 °C [54]).

The different values of X were obtained from runs 4 and 7 conducted at 700 °C using the $CaCl_2$–NaCl and molten LiCl electrolytes. It was found that the Al_2O_3 tube was reduced at 700 °C, with $X = 35\%$ obtained after 23.33 h electrolysis in the $CaCl_2$–NaCl melt (run 4) as opposed to $X = 71\%$ at 900 °C in run 3. It was, however, observed that no electro-deoxidation of the Al_2O_3 took place in the molten LiCl at 700 °C (run 7). Two main causes were considered to be responsible for the latter observation. First, at lower temperatures, probably 700 °C or less, there are increasing effects of mass transport constraints on the O to be ionized from insulating solid Al_2O_3, hence the very sluggish kinetics of oxygen transport within the Al_2O_3 lattice and consequently solid-state cathodic oxygen ionizations from the Al_2O_3 at the 3PBs of Al_2O_3/LiCl/Nb. The diffusivity of oxygen in α-Al_2O_3 is very low and it decreases drastically with decreasing temperature, e.g., from about 2.2×10^{-22} $m^2\ s^{-1}$ at 1,400 °C down to 1.1×10^{-24} $m^2\ s^{-1}$ at 1,200 °C [55]. As to the formation of $LiAlO_2$ on the Al_2O_3 surface, unfortunately, there are so far no activity coefficients ($\gamma_{(Li_2O)}$) of Li_2O dissolved in molten LiCl available in the literature. It is thus difficult to estimate initial O^{2-} activity (i.e., pO^{2-}) in the LiCl melt and predict the $LiAlO_2$ formation at 700 °C. Also, any change in the Al_2O_3 mass before and after electrolysis was not measurable. Second, even if a thin layer of $LiAlO_2$ forms on the Al_2O_3 surface, $LiAlO_2$ is much more stable than the Ca aluminates as evident from Fig. 3a. As discussed previously, $LiAlO_2$ is even thermodynamically more stable than molten LiCl over the pO^{2-} region of 0–2.2 at 700 °C. It is thus difficult for cathodic ionization of the oxygen from the $LiAlO_2$ to occur in the LiCl melt at 700 °C.

Overall, the present results reveal that the $CaCl_2$–NaCl electrolyte is more suitable than the equimolar $CaCl_2$–LiCl electrolyte in terms of Al purity. Although molten $CaCl_2$ or LiCl has appreciable solubility for O^{2-}, the use of $CaCl_2$ as the main electrolyte component appears to facilitate the electro-deoxidation of Al_2O_3 more effectively than LiCl.

3.4.3 *Effect of electrolysis temperature*

It is well known that fused salt electrolysis at low temperatures may offer a number of advantages, e.g., lower corrosive damage to the cell vessel, lower loss of electrolyte due to vaporization, and wide availability of materials for electrodes and cell linings. Attempts were therefore made to conduct the electrolytic reduction of solid Al_2O_3 at 700 °C (runs 4–9).

For the $CaCl_2$–NaCl melt containing 32.2 mol% NaCl, the value of X for run 4 conducted at 700 °C was 35% and was about half of that achieved for run 3 at 900 °C. The observed increase in X with increasing temperature can mainly be ascribed to decreasing stability of the oxides in the electrolyte, as evident from Fig. 2, and enhanced kinetics of Reactions 6 and 7.

However, when using the equimolar $CaCl_2$–LiCl electrolyte, the value of $X = 100\%$ was obtained from run 5 after electrolysis at 700 °C, whereas the value of X was 78% for run 2 using the same electrolyte at 900 °C. Complete reduction was repeated by conducting run 6 under almost the same conditions as run 5. For both runs 5 and 6, the cathode product was Al_2Ca only, free of any oxides, whereas the products from run 2 at 900 °C were metallic Al with 5.4 at% dissolved Ca and the un-reduced oxides. Liu and Poignet reported that Li activities increase with decreasing temperature at temperatures between 650 and 800 °C for dilute solutions of Li in Li–LiCl melts [56]. Therefore, the activities of Li and Ca dissolved in the $CaCl_2$–LiCl melt become larger as the melt temperature

decreases because of increasing Li activity and consequently Ca activity through Reaction 14 with decreasing temperature. A comparison in iso-activity lines of Ca for the Al/Al_2Ca equilibrium between 700 and 900 °C in Fig. 3 reveals that the activity of the Ca dissolved in the electrolytes needed to form Al_2Ca at 700 °C is much lower than that at 900 °C, suggestive of the easier formation of Al_2Ca at 700 °C than 900 °C. This prediction is consistent with the findings from runs 2 and 5 or 6. The findings also indicate that the activities of Ca dissolved in the equimolar $CaCl_2$–LiCl melt had exceeded the value for Al_2Ca to be thermodynamically stable at 700 °C and were below the value for Al_2Ca to be stable at 900 °C, which explains the formation of Al_2Ca in the cathode product at 700 °C but not at 900 °C. The observed faster reduction rates at 700 °C compared to 900 °C probably result from a small degree of contributions from chemical reduction of the Al_2O_3 by the dissolved Ca and Li.

To clarify possible involvement of metallothermic reduction in the overall reduction process, especially at low temperatures, electrolysis was carried out in a Li-saturated Li–LiCl electrolyte at 700 °C (runs 8 and 9). It was found that the reduction of the Al_2O_3 occurred, with the reduction extent increased and the reduction rates decreased with time. It should be mentioned that, in a Li-saturated LiCl–Li melt, the electronic conductivity of the melt is very high and very little ionic transfer occurs in the melt. Any contributions from electro-deoxidation of the Al_2O_3 to the overall reduction might be limited. As a result, the observed reduction can be mainly attributed to the reaction:

$$\begin{aligned} &Al_2O_3 + 6(Li) = 2Al + 3(Li_2O) \\ &\Delta G^{\circ}_{973K} = -36.379\,\text{kJ mol}^{-1}\,[41] \end{aligned} \quad (15)$$

The experimental results indicate that the chemical reduction of the Al_2O_3 by the Ca and Li dissolved in $CaCl_2$–LiCl melt might be involved in the overall reduction process provided that the activities of Ca and Li dissolved in the melt are increased significantly.

This study shows that the in situ formation of the electronically conducting oxides on the Al_2O_3 surface, determined by O^{2-} activities in the electrolytes, is essential for the electro-deoxidation of solid Al_2O_3 to continue. The O^{2-} activities and thermodynamic stabilities of the oxides are closely related to the salt systems used and appear to be important in determining observed reduction behaviour and Ca contents of the reduced Al. The Al metal with small amounts of Ca produced can be directly used as the deoxidant for the production of steel and Ti aluminides or as the master alloys for the production of various advanced alloys containing Al and Ca constituents [57, 58]. This may be economically attractive because of the higher prices of Ca than Al. Alternatively, high-purity Al can be produced from the present products using existing melt purification techniques, such as chlorination, which is being utilized for the efficient removal of Na from Al metal produced by the Hall–Heroult process.

4 Conclusions

Solid Al_2O_3 was reduced electrolytically to Al metal in molten $CaCl_2$–NaCl and $CaCl_2$–LiCl electrolytes, respectively, at an applied potential of 3.1 V and at 900 °C. It was found that the overall rates of direct electrolytic reduction of the solid Al_2O_3 were little influenced by the electrolyte systems used at 900 °C. It was also found that lower concentration of Ca in the reduced Al was obtained with molten $CaCl_2$–NaCl electrolyte compared to that with $CaCl_2$–LiCl electrolyte. The Ca aluminates were formed as the main intermediate reaction products and were subsequently reduced electrolytically to form Al-rich Al–Ca alloys during the course of electrolysis, which was partly responsible for the presence of Ca in the Al produced. The formation of Al–Ca alloys was likely to be caused by Ca being produced at reduced activity at the cathode surface and dissolving in the molten Al. The experimental observations were consistent with the thermodynamic predications using E-pO^{2-} diagrams of Al in the electrolytes at 700 and 900 °C.

Acknowledgments The authors gratefully acknowledge the Light Metals Flagship, a National Research Program of Australia, for financial support. Mrs. N. A. Olshina is thanked for conducting XRD analyses of the samples. Characterization of the samples using the SEM-EDS and EDX by Mr. D. J. Cameron and Dr. A. M. Glenn is appreciated. Assistance from the Analytical Services Group of CSIRO Minerals at Clayton is also acknowledged. Finally, the authors would like to thank the reviewer for the valuable comments that were considered in revising and improving our manuscript.

References

1. Grjotheim K, Welch BJ (1988) Aluminium smelter technology. Aluminium-Verlag, Dusseldorf
2. Kirk-Othmer (2002) Encyclopaedia of chemical technology, vol 2. Wiley, New York, p 279
3. Fray DJ (1988) In: Sohn HY, Geskin ES (eds) Metallurgical processes for the year 2000 and beyond. TMS, Warrendale, PA, p 493
4. Edwards L, Kvande H (2001) J Met 53:28
5. Welch BJ, Hyland MM, James BJ (2001) J Met 53:13
6. Tabereaux AT (1992) J Met 44:20
7. Choate WT, Green JAS (2003) U.S. energy requirements for aluminum production: historical perspective, theoretical limits and new opportunities. U.S. Department of Energy, Energy Efficiency and Renewable Energy, Washington, DC
8. Cochran CN (1987) Production of aluminium by alternate processes. In: 8th international light metals congress, Leoben, Vienna, p 82
9. Fray DJ, Farthing TW, Chen Z (1998) International patent PCT/GB99/01781, first filing date, 05 June
10. Chen GZ, Fray DJ, Farthing TW (2000) Nature 407:361

11. Fray DJ (2000) Metall Mater Trans B 31B:1153
12. Fray DJ (2001) J Met 53:26
13. Fray DJ (2002) Can Metall Q 41:433
14. Yan XY, Fray DJ (2002) Metall Mater Trans B 33B:685
15. Nohira T, Yasuda K, Ito Y (2003) Nat Mater 2:397
16. Jin XB, Gao P, Wang DH, Hu XH, Chen GZ (2004) Angew Chem 116:751
17. Yan XY, Fray DJ (2005) J Electrochem Soc 152:D12
18. Yan XY, Fray DJ (2005) J Electrochem Soc 152:E308
19. Qiu GH, Ma M, Wang DH, Jin XB, Hu XH, Chen GZ (2005) J Electrochem Soc 152:E328
20. Schwandt C, Fray DJ (2005) Electrochim Acta 51:66
21. Sakamura Y, Kurata M, Inoue T (2006) J Electrochem Soc 153:D31
22. Yan XY, Fray DJ (2005) Adv Funct Mater 15:1757
23. Jiang K, Hu XH, Ma M, Wang DH, Qiu GH, Jin XB, Chen GZ (2006) Angew Chem 118:442
24. Wenz DA, Johnson I, Wolson RD (1969) J Chem Eng Data 14:252
25. Story JB, Clarke JT (1957) J Met 9:1449
26. Littlewood R (1962) J Electrochem Soc 109:525
27. Ferry DM, Picard GS, Tremillon BL (1988) Trans IMM C 97:C21
28. Martinez AM, Castrillejo Y, Barrado E, Harrberg GM, Picard G (1998) J Electroanal Chem 449:67
29. Dring K, Dashwood R, Inman D (2005) J Electrochem Soc 152:D184
30. Dring K, Bhagat R, Jackson M, Dashwood R, Inman D (2006) J Alloys Comp 419:103
31. Bhagat R, Jackson M, Inman D, Dashwood R (2008) J Electrochem Soc 155:E63
32. Yasuda K, Nohira T, Hagiwara R, Ogata YH (2007) J Electrochem Soc 154:E95
33. Picard G, Seon F, Tremillon B (1980) Electrochim Acta 25:1453
34. Picard G, Seon F, Tremillon B (1983) Selective chlorination of oxides in suspension in molten chlorides. In: Proceedings of 1st inter symposium on molten salt chemistry and technology, Kyoto, p 49
35. Tremillon B, Picard G (1987) In: Mamantov G, Mamantov R (eds) Molten salt chemistry. D Reidel Publishing Company, Boston, MA, p 305
36. Boghosian S, Godo A, Mediaas H, Ravlo W, Ostvold T (1991) Acta Chem Scand 45:145
37. Stern KH, Panayappan R, Flinn DR (1977) J Electrochem Soc 124:641
38. Janz GJ (1967) Molten salts handbook. Academic Press, New York, p 180
39. Roth RS (ed) (2001) Phase equilibria diagrams, vol XIII. The American Ceramic Society, Ohio, p 84
40. Chartrand P, Pelton AD (2001) Metall Mater Trans A 32A:1361
41. HSC (1999) Outokumpu chemistry for windows, version 4.0, Outokumpu Research Oy Information Service, Pori, Finland
42. Johnson GK, Pierce RD, Poa DS, McPheeters CC (1994) In: Mishra B, Averill WA (eds) Actinide processing: methods and materials. TMS, Warrendale, PA, p 199
43. Wang SL, Zhang FH, Liu XA, Zhang LJ (2008) Thermochim Acta 470:105
44. Cowley WE (1982) In: Lovering DG (ed) Molten salt technologies. Plenum Press, New York, p 57
45. Haarberg GM, Thonstad J (1989) J Appl Electrochem 19:789
46. Shackelford JF, Alexander W (2001) CRC Materials science and engineering handbook, 3rd edn. CRC Press, FL, p 565
47. Okamoto H (2003) J Phase Equilib 24:91
48. Matsuishi S, Toda Y, Miyakawa M, Hayashi K, Kamiya T, Hirano M, Tanaka I, Hosono H (2003) Science 301:626
49. Kim SW, Matsuishi S, Nomura T, Kubota Y, Takata M, Hayashi K, Kamiya T, Hirano M, Hosono H (2007) Nano Lett 7:1138
50. Medvedeva JE, Teasley EN, Hoffman MD (2007) Phys Rev B 76:155107
51. Sharma RA (1970) J Phys Chem 74:3896
52. Bredig MA, Johnson JW, Smith WT (1955) J Am Chem Soc 77:307
53. Nakajima T, Minami R, Nakanishi K, Watanabe N (1974) Bull Chem Soc Jpn 47:2071
54. Murray JL (1983) Bull Alloy Phase Diagr 4:137
55. Heuer AH, Lagerlof KPD (1999) Phil Mag Lett 79:619
56. Liu J, Poignet JC (1990) J Appl Electrochem 20:864
57. Kirk-Othmer (1992) Encyclopedia of chemical technology, 4th edn. Wiley, New York, p 783
58. Ozturk K, Zhong Y, Luo AA, Liu ZK (2003) J Met 55:40